Initial Lunar Calibration Observations by the EO-1 Hyperion Imaging Spectrometer

Hugh H. Kieffer[a] , Peter Jarecke[b] and Jay Pearlman[b]

[a] U.S. Geological Survey, 2255 N. Gemini Drive, Flagstaff AZ, 86001
[b] TRW, Space Systems Division, One Space Park, Redondo Beach CA, 90278

ABSTRACT

The Moon provides an exo-atmospheric radiance source that can be used to determine trends in instrument radiometric responsivity with high precision. Lunar observations can also be used for absolute radiometric calibration; knowledge of the radiometric scale will steadily improve through independent study of lunar spectral photometry and with sharing of the Moon as a calibration target by increasing numbers of spacecraft, each with its own calibration history. EO-1 calibration includes periodic observation of the Moon by all three of its instruments. Observations are normally made with a phase angle of about 7 degrees (or about 12 hours from the time of Full Moon). Also, SeaWiFS has been making observations at such phase angles for several years, and observations of the Moon by instrument pairs, even if at different times, can be used to transfer absolute calibration. A challenge for EO-1 is pointing to include the entire full Moon in the narrow Hyperion scan. Three Hyperion observations in early 2001 covering an order-of-magnitude difference in lunar irradiance show good agreement for responsivity; the SWIR detector has undergone some changes in responsivity. Small discrepancies of calibration with wavelength could be smoothed using the Moon as a source. Off-axis scattered light response and cross-track response variations can be assessed using the lunar image.

Keywords: Moon, calibration, spacecraft

1. INTRODUCTION

The advantages and complications of using the Moon as a calibration target for Earth-orbiting spacecraft have been previously discussed.[1–5] The intrinsic stability of the lunar surface photometric properties[6] means that a lunar radiometric model, once established, can be applied to observations made at any time. A corollary is that observations of the Moon made by the same or different spacecraft at diverse times can be inter-compared through use of a lunar radiometric model. This has the potential of interrelating the calibration scales of all spacecraft which view the Moon. The launch of EO-1, with two multi-band imaging systems and the Hyperion imaging spectrometer, provides the opportunity to test several lunar calibration concepts. This work will concentrate on Hyperion observations and includes a comparison with SeaWiFS lunar observations.

Both SeaWiFS and Hyperion normally view the Moon with the phase angle (Sun-Moon-spacecraft angle) near $\pm 7°$(phase angle is strictly a positive quantity, however it is convenient to use negative values to distinguish observations made before full Moon). These phase angles catch the Moon near its maximum brightness, but avoid both eclipse phenomena and the radiance uncertainties associated with the Moon's strong and narrow backscatter peak.

The apparent diameter of the Moon (expressed in nominal nadir km) ranges from 6.2 (at apogee) to 6.8 km (perigee) for the nominal EO-1 orbit. The Hyperion push-broom imaging spectrometer has a nominal 7.5 km cross-track swath (0.623° field of regard), which allows little tolerance for getting coverage of the entire Moon. Hyperion has captured the entire illuminated Moon thus far only for a half-Moon observation.

Complete lunar images can be compared directly with models of lunar irradiance to generate instrument gain factors. Because the Moon is variegated, radiometric analysis of partial lunar images properly requires comparison to a spatially-resolved lunar radiometric model, which is being developed from an Earth-based observing program.[2,7] For now, a simple area factor is used; this implicitly assumes that the average brightness in the missing portion is the same as in the imaged portion. In addition to radiometric calibration, lunar images can be used for determination of off-axis scattered light sensitivity.

Further author information: (Send correspondence to H.H.K.)
E-mail: hkieffer@usgs.gov; telephone: 520-556-7015; fax: 520-556-7014 520-779-3761
P.J.: e-mail: Peter.Jarecke@trw.com J.P.: e-mail: Jay.Pearlman@trw.com

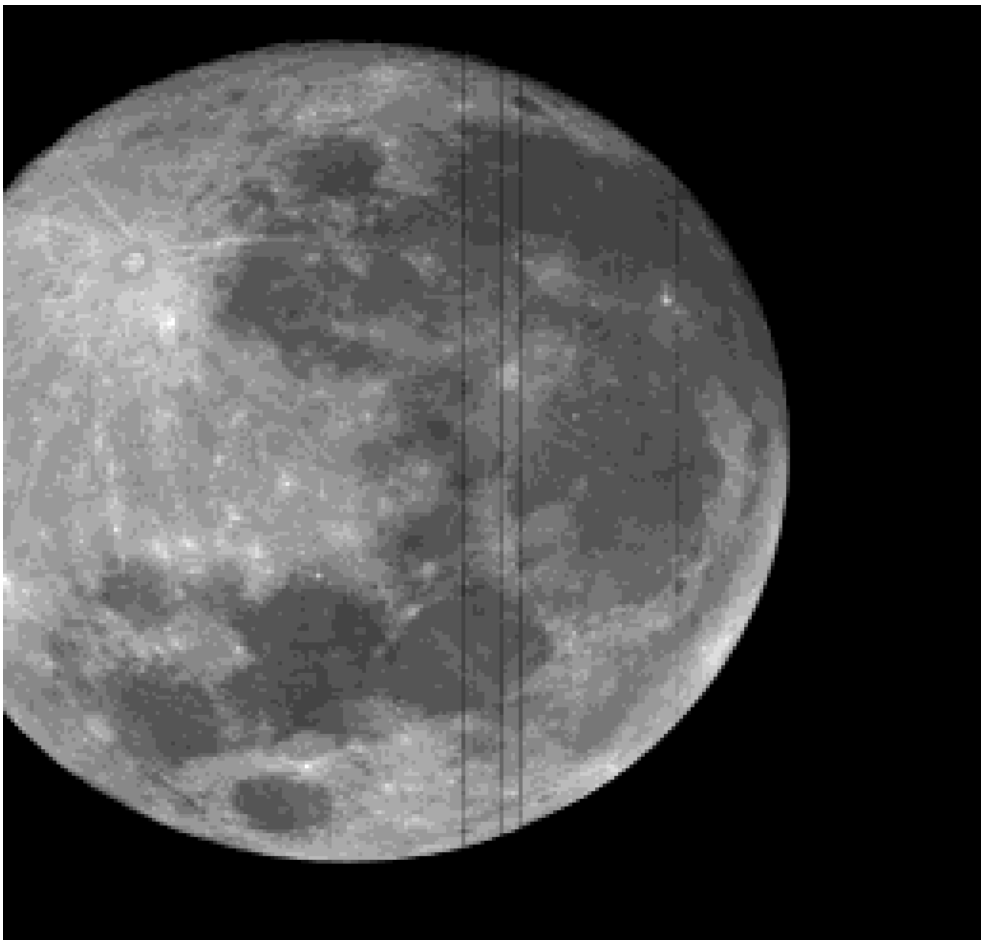

Figure 1. Day 38 image of the Moon. Every 9th frame of Band 39 in a Level 0.5 image was used to recover approximately a round Moon. Lunar north is toward 4 o'clock. Hyperion frame numbers increase upward, column numbers increase to the right. The three strong stripes are locations of straps on the VNIR detector and are accounted for in the calibration.

2. HYPERION LUNAR OBSERVATIONS

Beginning in 2001 January, the EO-1 spacecraft has attempted lunar observations about once per month. Because of the multiple detector arrays on EO-1 and their differences in pointing directions, compromises in pointing are involved; Hyperion obtained useful lunar observations in 2001 February, April, and June; observations through April are discussed here. Geometric values for these observations are given in Table 1.

Lunar scans are accomplished by re-orienting the spacecraft from pointing toward the center of the Earth to pointing near the Moon; this maneuver begins roughly when the spacecraft enters the Earths' shadow near the South Pole. Then a few slow pitch maneuvers of alternating direction are done, with intervening small rolls, such that the Moon traces out a boustrophedonic raster pattern over the instrument focal planes, with the Moon going a degree or so beyond the detector on each pitch. The pitch rates are set so that the angular velocity of the Moon past the detector is roughly 8 times slower than the angular velocity of a normal nadir scene, leading to an oversampling factor of about 8. On alternate months, one scan is aimed to pass over the center of the Hyperion detector. A typical image of the Moon in one Hyperion band is shown in Fig. 1.

3. GENERIC PROCESSING OF SPACECRAFT IMAGES FOR LUNAR CALIBRATION

In the simplest lunar calibration method, spacecraft observations of the Moon are reduced to observed irradiance, corrected to standard distance, and compared with the irradiance predicted for each band at standard distance and the same illumination and observing geometry.

3.1. Image processing overview

- Determine the average "dark" (zero-incident radiance) Data-Number (N) for each detector(i) in each band(b); $\equiv \langle N_d \rangle_{bi}$. Subtract these from all lunar image frames.
- Determine the location and extent of the Moon in each image, which includes the semi-major and semi-minor axes, R_y and R_x of an ellipse that best fits the limb of the Moon (the inflection points in the rise of brightness onto the Moon at a lit edge, this is roughly where the second derivative is zero). In instruments for which the pixels are the same size in each band and are strictly coincident, these could be averaged over band.
- Determine the region of each image to be summed to represent the Moon. This will be a compromise between a margin around the Moon to account for instrument MTF and uncertainty in N_d. Use of an elliptical region is preferred.
- Compute the calibrated radiance of each pixel; j is the pixel index orthogonal to i:

$$\Re_{b_{ij}} = (N_{i,j,b} - \langle N_d \rangle_b) \cdot C_{i,j} \tag{1}$$

  where $C_{i,j}$ is the radiometric calibration of each detector element in radiance per data-number. If there is only one detector per band (e.g., SeaWiFS), radiometric calibration can be delayed to a later step.

- Replace any bad pixels by an appropriate interpolation of the values for neighboring good pixels, e.g., as described by Kieffer.[8]
- Sum the calibrated radiance of the Moon;

$$\Re_b \equiv \sum_{i,j} \Re_{b_{ij}} \tag{2}$$

3.2. Geometric processing overview

- Process the geometric information to calculate position of the Sun, Moon and viewer (spacecraft) and the orientation of the Moon in a consistent coordinate system(e.g., J2000). From these, calculate the distance from the viewer to the Moon in km, $D_{\oslash}$; the distance of the Moon from the Sun in Astronomical Units, $D_{\odot}$; the sub-solar and sub-viewer selenographic latitudes θ and longitudes ϕ, and the phase angle $g = \cos^{-1}(\frac{\overline{\bowtie\oslash}\cdot\overline{\odot\oslash}}{|\overline{\bowtie\oslash}|\ |\overline{\odot\oslash}|})$ where $\overline{\bowtie\oslash}$ is the vector from the Moon to the viewer and $\overline{\odot\oslash}$ is the vector from the Moon to the Sun.
- Determine the expected angular radius of the Moon: $R_m = 1738/D_{\oslash}$
- Determine the expected radius of the Moon in pixels: $Y_o = R_m/P_y$, where P_y is the nominal angular size of a pixel in the Y direction, and similarly for X.
- Determine the oversampling factor for observation k, normally presumed to be the same for all bands:

$$W_k = Y_o/R_{yk}. \tag{3}$$

- Calculate the irradiance correction factor to standard distances:

$$f_k = D^2_{\odot k} \cdot \left(\frac{D_{\oslash k}}{384400}\right)^2 \tag{4}$$

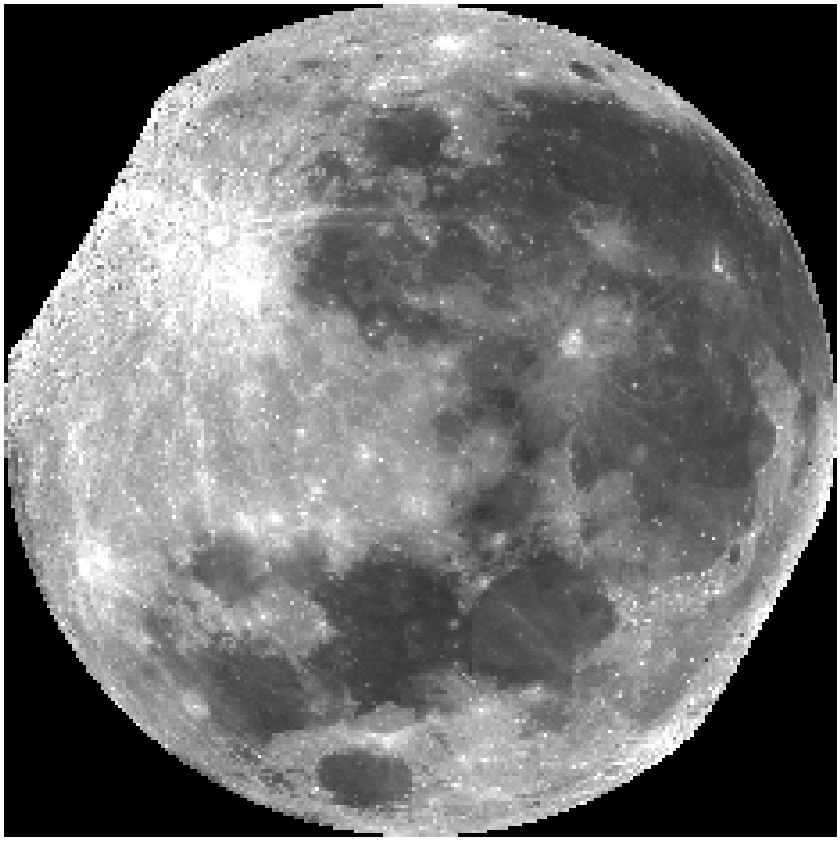

Figure 2. Reprojection of Clementine provisional mosaic to the viewing conditions by EO-1 on Day 38, Band B. The mosaic did not include latitudes greater than 70°. Because Clementine viewing is close to nadir, shadowed regions at high latitudes are weighted in proportion to their true area, not largely hidden as is the case for viewing at small phase angles. This image shows intrinsic reflection coefficient, not true brightness for the specific illumination conditions. The image is centered over -3.23°N, 0.12°W, and rotated 120° clockwise; it is 233 pixels in diameter to match the Hyperion Day 38 observation. Lunar north is toward 4 o'clock.

3.3. Radiometric processing overview

- Calculate the instrument-calibrated lunar irradiance at standard distance

$$\mathcal{I}_{\bowtie bk} = f_k \cdot \Re_{bk} \cdot \Omega_p / W_{bk}, \tag{5}$$

  where $\Omega_p = P_x P_y$ is the solid angle of one pixel.

- Evaluate a lunar radiometric model at the same geometry for the effective wavelength of a band λ_b. Although both the telescopic observations that form the basis of the ROLO lunar photometric model and spacecraft images of the Moon are processed as radiance, the development of coefficients in the model is done in dimensionless units of reflectance. The conversion between irradiance and effective disk reflectance is:

$$\mathcal{I}_{\oslash \lambda_b} = A_{\oslash \lambda_b} \cdot \Omega_{\oslash} S_{\odot \lambda} / \pi \tag{6}$$

  where $A_{\oslash}$ is the disk-equivalent albedo, λ is the effective wavelength of a band, $\Omega_{\oslash}$ is the solid angle of the Moon and $S_{\odot}$ is the solar spectral irradiance, the last two both at standard distance. This conversion involves a solar spectral irradiance model, which may have significant uncertainties in some wavelength regions. However, the direct dependence on solar model cancels to first order as long as the same model is used in going from irradiance to reflectance and back.

- Compare the measured irradiance to the model irradiance. The calibration discrepancy for band b and observation k is:

$$\mathcal{I}_{\bowtie bk}/\mathcal{I}_{\oslash \lambda_b k} - 1 \tag{7}$$

4. PROCESSING OF HYPERION DATA

The processing described here began with raw data apart from a "smear and echo" correction for electronics artifacts which had already been applied to the SWIR data; these are termed Hyperion "Level 0.5" files. These image cubes were processed through the steps described in Section 3, with some additional details.

- The lunar image cubes were dark-corrected using frames preceding crossing onto the Moon; then each frame of the dark-corrected cube was multiplied by the Hyperion response calibration file and an additional factor of 10 (to preserve precision) before converting back to integer format.
- A rectangle circumscribing the Moon in the image with about a 10 pixel extra size (or going to the edge of the frame) was averaged over the samples and frames for each band to generate an average radiance spectrum for the rectangle. The radiance average was multiplied by the number of samples and frames in the rectangle to get an image "intensity".
- When the illuminated Moon was not completely covered by the image, the image intensity was divided by the fraction of the Moon captured by the rectangle.
- The over-sample factor was determined by averaging R_y over all bands that had a good signal-to-noise ratio.

The Day 38 data supplied appeared to contain a scale difference of ∼13% in the SWIR from the other two days, thought to be associated with the smear and echo correction. The results shown here have had the Day 38 SWIR multiplied by 1.13.

4.1. Geometric processing details

EO-1 scans of the Moon pass from limb to limb in about 8 seconds. The middle time of this period is used for geometric calculations. Tables of EO-1 positions spanning these lunar observations at 1 second intervals were generated by the EO-1 project. The JPL double precision planetary ephemeris is used to compute the location of the Sun, the Earth-Moon barycenter relative to the barycenter of the solar system, and the geocentric location of the Moon, all in J2000 coordinates. The orientation of the Moon is based on the IAU equations and constants[9]; the orientation in the above ephemeris is virtually identical to this. The relative positions of the Sun, Moon and spacecraft are then used to compute distances and the apparent orientation of the Moon.

The pixel size is based on ground calibration of the Field of Regard; the average for the VNIR and SWIR systems is 42.466 micro-radian.

4.1.1. Determining location, size and shape of the lunar image

The location and shape of the lunar image in each band was determined by fitting an ellipse to the limb. This yields consistent results for bands with appreciable signal. As an example, the results for all bands which had a consistent convergence in the Day 38 image are shown in Figure 3 and Table 2.

For the Day 38 observation, the agreement in cross-track scale is 0.24%, even though the left limb was not observed.

4.1.2. Over-sampling factor

For a constant angular rotational velocity of the spacecraft, the apparent irradiance of the Moon depends linearly upon the length of time spent crossing it, or equivalently, upon the oversampling of the Moon in the line direction. This over-sampling factor can be derived from the size of the lunar images themselves; for high-resolution instruments, this is commonly more accurate than the engineering telemetry on the spacecraft pitch rate during a lunar maneuver.

Table 1. Hyperion Lunar Observation Geometry

Item	Day 33	Day 38	Day 97
Observation time, UT: year mon day	2001 Feb 2	2001 Feb 7	2001 Apr 7
" hr min sec	1 29 59	20 1 26	17 59 46
Spacecraft position: J2000 km, X	-1601.5	-1817.8	-6832.4
" Y	6899.2	6395.4	1703.1
" Z	121.0	2433.5	763.8
S/C selenographic latitude $\theta_{\bowtie}$	5.28	-3.23	-6.61
" longitude $\phi_{\bowtie}$	-8.43	0.12	4.15
Sun selenographic latitude $\theta_{\odot}$	-0.72	-0.89	-1.52
" longitude $\phi_{\odot}$	76.35	6.28	8.85
S/C-Moon distance, km	377584.9	350625.0	362119.6
Moon-Sun distance, AU	0.98578	0.98877	1.00361
Irradiance distance factor	0.937611	0.813415	0.893863
Phase angle	-84.87	-6.58	-6.91
Diameter of moon from S/C, mrad	9.2059	9.9137	9.5990
Expected diameter of moon, pixels	216.78	233.45	226.04
Image-derived diameter, samples	217.18	233.15	226.78
Image-derived diameter, frames	1832.7	1949.8	1861.8
Oversample factor	8.43	8.356	8.232
Illuminated area: fractional	1.0	0.933	0.975

Table 2. Hyperion Lunar image size and shape, Day 38, using every 5th line

Item	X center	Y center	X SMA	Y SMA
VNIR mean	89.357	229.733	116.340	195.064
VNIR StdDev	0.067	0.044	0.067	0.042
SWIR mean	90.177	229.641	116.555	195.091
SWIR StdDev	0.102	0.038	0.075	0.058
Delta mean	0.820	-0.092	0.215	0.027
Both StdDev	0.122	0.058	0.101	0.072

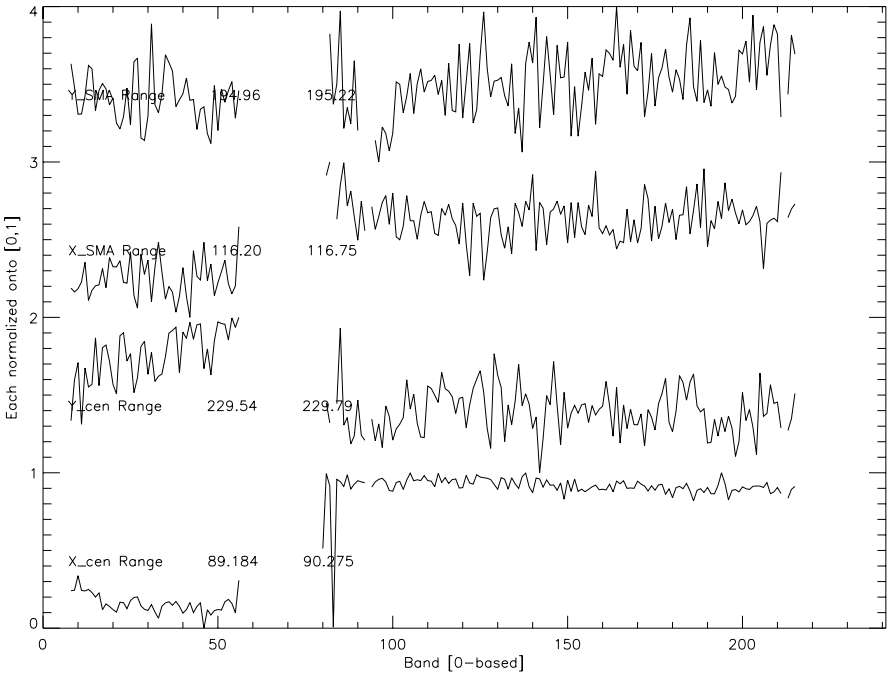

Figure 3. Location and size of the ellipse that best fits the Moon limb in the Day 38 dark-subtracted image using every 5th line. Results for bands with poor response have been eliminated. The four curves are individually scaled; the printed range indicates the minimum and maximum for each parameter; for the upper three curves, the scale is about 0.04 pixel per minor tick. X is the sample direction, Y is in the time (frame) direction; the lower two curves are the location of the Moon center, the upper two curves are the semi-major-axes. There is a small difference in X location between the VNIR and SWIR bands. The small trend in Y location within the VNIR may be due to spectral smile.

4.1.3. Corrections for partial coverage

For observations within a few degrees of full Moon, the image can be approximated as uniform disk. The geometric fraction of a disk of radius r which is omitted by coverage which extends only c from the center of the disk is $\left[\theta - \frac{\sin 2\theta}{2}\right]/\pi$ where $\theta = \cos^{-1}(c/r)$. This relation is used to correct for partial coverage; because the missing fractions are small for the Hyperion observations, the effect of lunar variegation is correspondingly diminished.

4.2. Individual detector element response

4.2.1. Bad elements

Using the raw image, a set of frames acquired of space before crossing onto the Moon is used to determine the Mean Absolute Second Difference (MASD) as a measure of detector noise. A 5-sigma test identifies the first element of bands 1 to 35. Using a space-subtracted image, the average response for all detector elements is computed for a set of frames straddling the middle of the Moon. An effective noise level is computed as the root-mean-square of the MASD for this central Moon and the MASD of space. For those columns that are on the Moon and for bands where the response is > 0.2 the average of all bands, the signal-to-noise ratio (SNR) is computed. Locations where the twice-normalized (over band and column) SNR is > 0.2 are labeled bad. Combining the Day 38 and Day 97 images identified 10 'dead' pixels (sample,band): (95,72),(93,94),(92,99),(138,116),(256,168),(23,169),(113,190),(8,200), (8,201),(115,203). The first sample in each of the first 35 bands is extremely noisy.

Bad pixels are replaced with the average of their left and right neighbors in each frame, or one neighbor if the point is on the array edge. A total of 39 out of 242 bands are ignored due to low spectral response; of the remaining bands, 37 out of 51,968 pixels, or 0.07%, are not usable.

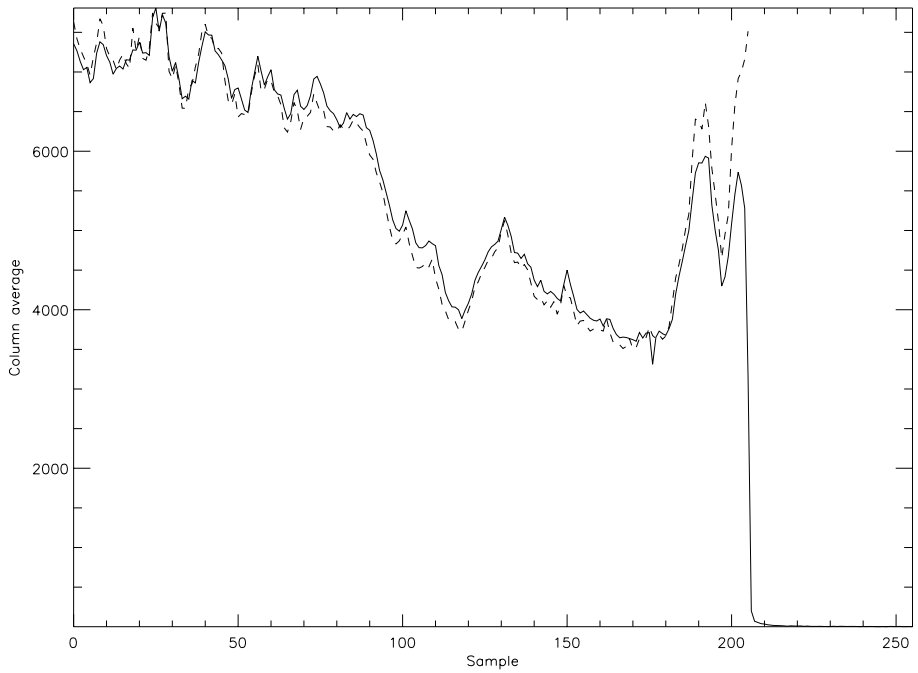

Figure 4. Cross-track profiles of the calibrated Day 38 Moon and Clementine images. A horizontal strip of about 30 frames was extracted from near the middle of the Hyperion image, and the corresponding region from the reprojected Clementine image (see Fig. 2). Both these strips were averaged over all lines. Although the Moon is variegated, the radiance patterns in the two images match closely, indicating that there is no significant cross-track calibration error in Hyperion. The divergence at the right edge is probably due in part to the extended response of Hyperion sensing space.

4.3. Spurious signals

The raw images display a weak left-right mirror symmetry "ghost" of up to 1% strength, particularly in bands 8-20. This is most easily seen in the half-Moon image from Day 33. The magnitude of the ghost varies between bands, even adjacent bands, and the ghost has reversed contrast in many bands.

In the VNIR and SWIR, the rightmost (highest) 6 columns contain a weak version of the image that falls just off the left side of the detector, not reversed.

The SWIR bands have an "echo" at about -10 samples from the primary signal; this appears as a weak second left-side edge of the Moon. This effect was quantified by normalizing the spectrum of a rectangular region extending 2 to 9 samples left of the limb of the Moon for a range of ± 9 frames around the center of the Moon to the corresponding area just within the limb. With this measure, the VNIR effect is $< 0.5\%$ and the SWIR effect is $\sim 6\%$, becoming indeterminate for outermost SWIR bands, where the response is weak.

In one image studied closely (day 38), when the Moon was being viewed one pixel in the detector array was consistently high by about 5180. For virtually all of these, the bits corresponding to 2^{10} and 2^{12} were inappropriately set on (adding 5120); only the lower of these might be generated by the in-flight hardware; probably both are generated in ground processing. A similar number of DN near $\pm 2^{15}$ occurred in nine locations; these must be generated in ground processing.

4.4. Cross-track response

Because radiance model images from the ground-based lunar calibration program are in a preliminary stage, an image of the Moon was made from Clementine data and reprojected to nearly agree with Hyperion viewing (see Figure 2). Clementine band B was used, which is centered at 750 nm and has a nominal bandwidth of 10 nm, corresponding closely to Hyperion band 40.

Because the Moon is clipped on one side of the Hyperion full Moon images acquired thus far, and the Clementine mosaic does not cover the poles, only a modest range of lines could be used to make a cross-track comparison of brightness. This line range was chosen to include as many samples as possible.

The cross-track strips were averaged over line and normalized, then offset according to the Moon location in the Hyperion image. The cross-track profiles are shown in Figure 4. The close correspondence, considering the coarseness of 1-pixel registration, indicates that the cross-track calibration is close to correct.

4.5. Off-axis response

The spread of the lunar image into space was estimated from the average signal in a set of concentric annuli along a bright-limb sector on the side of the Moon opposite the "echo", using the elliptical bin algorithm described by Kieffer and Aderson.[10] The response drops to 1% at a distance of 4.0 pixels for the VNIR and 4.3 for the SWIR; the response is decreased to 0.1% at a distance of 30 pixels in the VNIR and 20 pixels in the SWIR.

5. HYPERION MEASURES OF LUNAR IRRADIANCE

All the steps leading to Equation 5 were done for the Level 0.5 data (smear and echo-corrected only) using the pre-launch radiometric calibration. No correction for detector temperature was done. The resulting Hyperion measures of lunar spectral irradiance, corrected to standard distance, are shown in Fig. 5. The irradiance on Day 33, acquired when the Moon was near first quarter, is nearly an order of magnitude below those on Days 38 and 97, both of which were acquired near 7° phase angle.

The features at 1400 and 1800-1920 nm resemble strong water vapor absorption features, inverted. High spectral resolution reflectance measurements of lunar soils[11] are smooth across these wavelength regions*, thus we attribute these features to laboratory calibration errors. The excursions near 925 nm are probably due to the low response of both VNIR and SWIR at these wavelengths; there is also a significant water vapor band centered at 940 nm.

6. LUNAR RADIOMETRIC MODEL

A lunar irradiance model has been developed based upon extensive Earth-based telescopic observations of the Moon and stars.[2,7] The irradiance model has the form:

$$\ln A_{\lambda k} = \sum_{i=0}^{m} a_i |g|^i + \sum_{j=1}^{n} p_j g^{2j-1} + c_a \theta_{\bowtie} + c_b \phi_{\bowtie} \qquad + c_o (1/|g| - 1/c_g) \quad \text{for} \quad |g| < c_g \tag{8}$$

where g, $\theta_{\bowtie}$ and $\phi_{\bowtie}$ are the observer phase angle and selenographic latitude and longitude. The polynomial in absolute phase angle has m =3, and the asymmetry polynomial has n=3 (fifth degree). The opposition effect (strong backscattering) represented by the last term has a width set at $c_g = 8.5°$. The a, p and other c coefficients are fit independently for each band.

Although both the telescopic observations that form the basis of the lunar photometric model and spacecraft images of the Moon are processed as radiance, the development of coefficients in the lunar photometric model is done in dimensionless units of reflectance. The conversion between radiance and reflectance units is:

$$A_\lambda = \frac{\mathcal{I}_\lambda}{\Omega_\oslash S_{\odot\lambda}/\pi} \tag{9}$$

where A is the disk-equivalent albedo, $\Omega_\oslash$ is the solid angle of the Moon and $S_\odot$ is the solar spectral irradiance, the last two both at standard distance. This conversion involves a solar spectral irradiance model, which may have significant uncertainties in some wavelength regions. However, the direct dependence on solar model cancels to first order as long as the same model is used in going from irradiance to reflectance and back. For the lunar model, the WCRP solar model[12] has been used throughout to date for consistency.

The model produces lunar irradiance at standard distance: $L_{\oslash k}$ (Sun-Moon = 1 A.U.,Observer-Moon = 384,400 km). The specific coefficients used here are based on calibration against the stellar color-magnitude system, with small corrections as a function of wavelength to agree with the reflectance spectra of Apollo returned samples measured in

*A spectrum is available at http://www.planetary.brown.edu/pds/AP62231.html

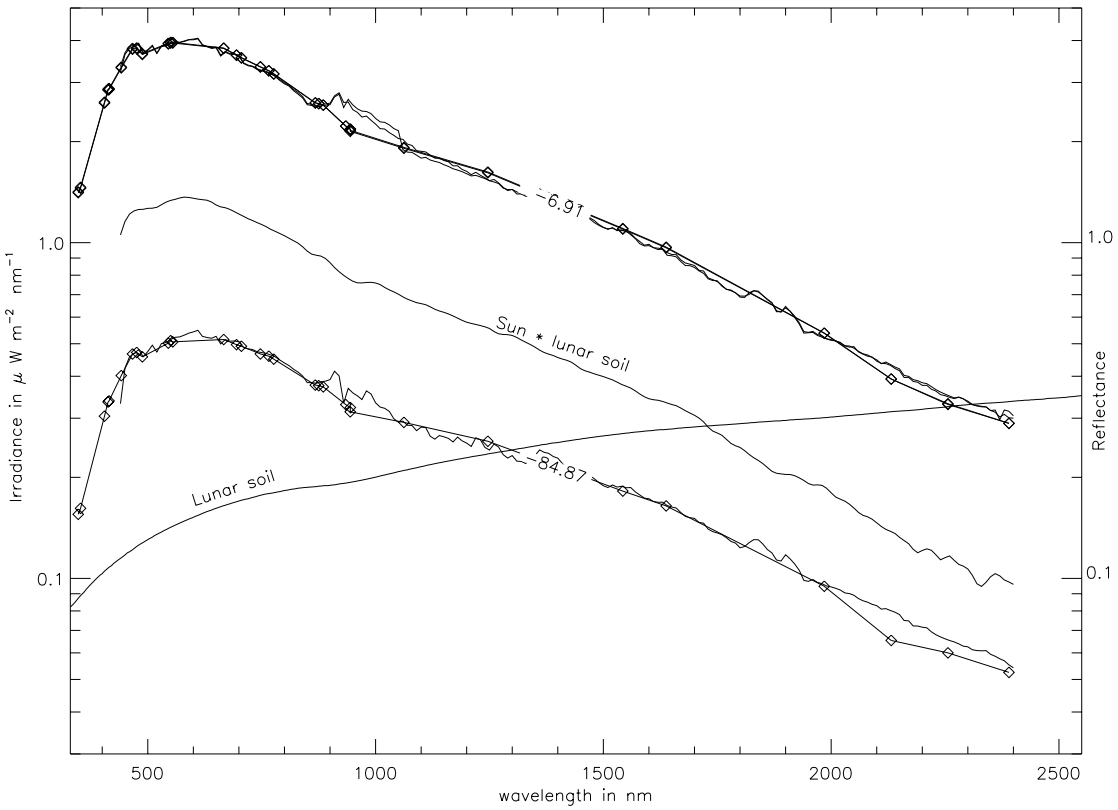

Figure 5. Lunar irradiance derived from Hyperion images and from a lunar radiometric model. Data are shown for the Day 33 (single lower curve), Day 38 and Day 97 (upper curves) observations. The SWIR values for Day 38 are roughly 10% low relative to Day 97. Outside of 440 nm to 2400 nm, the Hyperion calibration values are zero; the switch from the VNIR to the SWIR detectors in the wavelength overlap regions was set at 925nm. The diamonds are the predicted ROLO irradiance model. The curve rising in wavelength is the laboratory reflectance spectrum of a mature lunar soil from the Apollo 16 mission. The central curve is this spectrum multiplied by the WCRP solar spectrum filtered with a Gaussian form of half-width 10 nm at the Hyperion wavelengths.

the laboratory.[13] All work thus far has ignored variation with time of the solar spectral irradiance; the variation of total solar irradiance is about 0.1%,[14] although variation in the ultraviolet is considerably greater.

Because the Moon's spectral features are broad and shallow, linear wavelength interpolation in reflectance should be a reasonable first-order approach to comparing observations made in moderately different bands; that approach is used here.

7. ABSOLUTE IRRADIANCE COMPARISONS

The spectral irradiance of the Moon derived from Hyperion observations using the pre-launch calibration is compared to the predictions of the lunar irradiance model in Fig. 5.

SeaWiFS has made observations of the Moon on a monthly basis, usually near a phase angle of 7.5° in both waxing and waning phases. Barnes and McClain[15] have produced a calibration wherein the time-dependent terms are based on SeaWiFS lunar observations and a lunar model based on observations by Lane and Irvine[16] and a generalized photometric model.[17] Beginning with SeaWiFS raw images, the measured lunar irradiance is computed using the steps outlined in Section 3. The lunar irradiance model was then computed for the specific geometry of each SeaWiFS observation and the calibration discrepancy averaged over the first 20 observations.

Because of the strong dependence of lunar irradiance on geometric angles, observations by two spacecraft cannot be directly compared (barring the unlikely circumstance of simultaneous observations from similar locations). Rather,

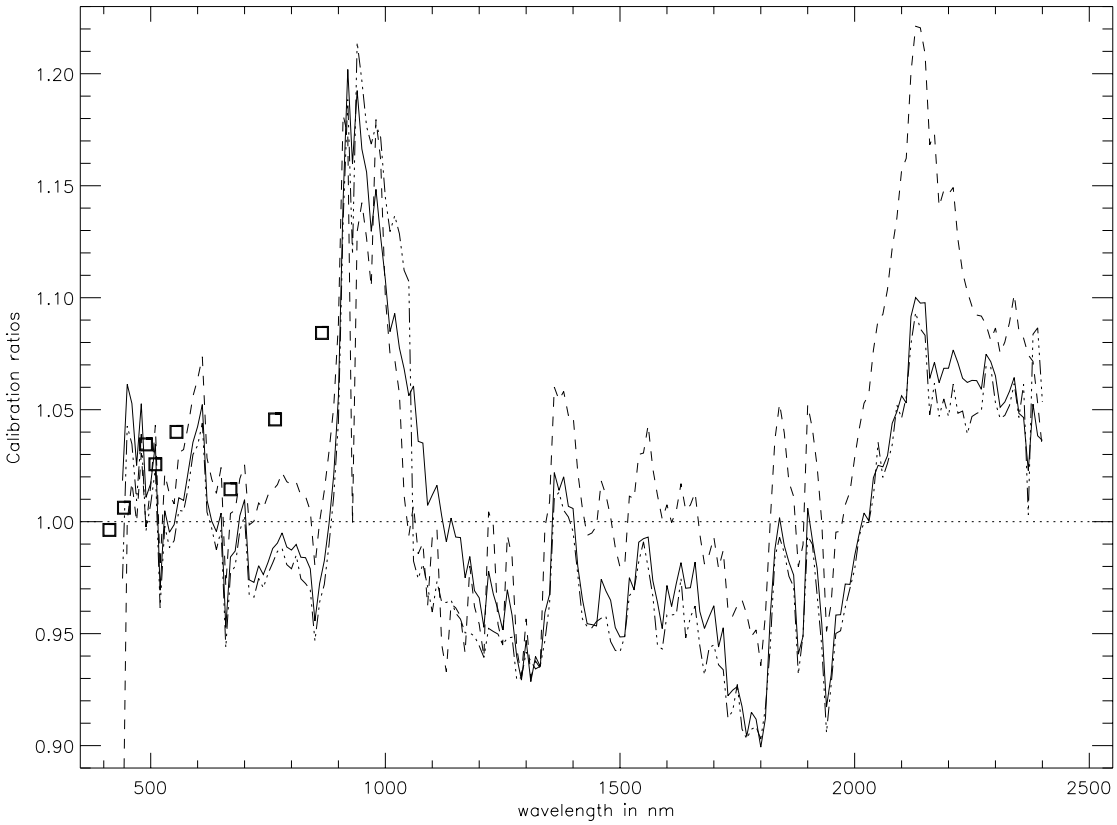

Figure 6. Comparison of derived lunar irradiances. The boxes are the ratio of the average of the first 20 SeaWiFS observations using the calibration described by Barnes and McClain[15] to the ROLO model. The three curves labeled are the ratios of Hyperion to the model for the appropriate phase angle and libration; the dashed curve is Day 33, the dash-triple-dot curve is Day 38, and the solid curve is Day 97.

the lunar irradiance based on each spacecraft instrument calibration can be compared with the lunar radiometric model in a way that the absolute radiometric scale in each ROLO band cancels.

The calibration of Hyperion and SeaWiFS relative to the lunar irradiance model is detailed in Figure 6. The SeaWiFS lunar irradiances are within about 3% of Hyperion for bands below 700nm; longer-wavelength SeaWiFS bands (Bands 7 and 8) are 5-10% higher than Hyperion; these two bands have shown a significant loss of response since launch.[4]

The Hyperion VNIR responsivity has remained constant to within about 1%. The SWIR responsivity may have dropped about 4% between Day 33 and Day 97; the absolute values for Day 38 are unreliable because of the uncertain pedigree of the data file as mentioned in Section 4.

The rapid oscillations in calibration ratio between 440 and 550 nm appear to be caused by use of a piecewise-linear pre-launch calibration curve. The oscillations between 600 and 800 nm also are most likely due to the instrument calibration coefficients. In this instance, it would be an improvement to use the lunar observations to adjust the calibration coefficients with respect to wavelength to yield a smooth spectrum of the Moon.

ACKNOWLEDGMENTS

We appreciate the efforts of Pamela Barry, Pamela Clancy, Momi Ono and Carol Segal to extract, prepare and deliver the Hyperion lunar images. Seth Shulman provided EO-1 absolute spacecraft positions at the time of lunar observations. Discussions with Stuart Frye, Paul Sanneman and Bruce Trout about the spacecraft attitude control system and maneuver design were very helpful. SeaWiFS data were provided by Gene Eplee. The ROLO project

is supported by Goddard Space Flight Center as part of the NASA Mission to Planet Earth under NASA contract S-41359-F.

REFERENCES

1. H. H. Kieffer and R. L. Wildey, "Absolute calibration of Landsat instruments using the Moon," *Photogramm. Eng. Remote Sens.* **51**, pp. 1391–1393, 1985.
2. H. H. Kieffer and R. L. Wildey, "Establishing the Moon as a spectral radiance standard," *J. of Atmospheric and Oceanic Technology* **13**(2), pp. 360–375, 1996.
3. R. A. Barnes, J. R. E. Eplee, and F. S. Patt, "SeaWiFS measurements of the Moon," *Proc. SPIE* **3438**, pp. 311–324, 1998.
4. R. A. Barnes, J. R. E. Eplee, F. S. Patt, and C. R. McClain, "Changes in the radiometric response of SeaWiFS determined from lunar and solar-based measurements," *Ap. Opt* **38**, pp. 4649–4664, 1999.
5. I. Grant, H. H. Kieffer, and J. M. Anderson, "Lunar calibration of geostationary visible-band images," *Proc. SPIE* **3438**, pp. 337–347, 1998.
6. H. H. Kieffer, "Photometric stability of the lunar surface," *Icarus* **130**, pp. 323–327, 1997.
7. J. M. Anderson, H. Kieffer, and K. Becker, "Modeling the brightness of the Moon over 350-2500 nm for spacecraft calibrations," *Proc. SPIE* **4169**, pp. 248–259, 2000.
8. H. H. Kieffer, "Detection and correction of bad pixels in hyperspectral sensors," *Proc. SPIE* **2821**, pp. 93–108, 1996.
9. M. E. Davies, V. K. Abalkin, A. Brahic, M. Bursa, B. H. Chovitz, J. H. Lieske, P. K. Seidelmann, A. T. Sinclair, and Y. S. Tjuflin, "Report of the IAU/IAG/COSPAR working group on cartographic coordinates and rotational elements of the planets and satellites: 1991," *Celestial Mechanics and Dynamical Astronomy* **53**, pp. 377–397, 1992.
10. H. H. Kieffer and J. A. Anderson, "Use of the Moon for spacecraft calibration over 350–2500 nm," *Proc. SPIE* **3438**, pp. 325–335, 1998.
11. C. M. Pieters, "The Moon as a calibration standard enabled by lunar samples," *in: New Views of the Moon II: Understanding the Moon through the Integration of Diverse Datasets. Flagstaff, AZ. Lunar and Planetary Instit. Contrib.* **980**, pp. 47–48, 1999.
12. C. Wehrli, "Spectral solar irradiance data." World Climate Research Program (WCRP) Publication Series No. 7, WMO ITD-No. 149, 1986. pp 119-126.
13. T. C. Stone, H. H. Kieffer, and J. M. Anderson, "Status of use of lunar irradiance for on-orbit calibration," *Proc. SPIE* **4483**, pp. xxx–xxx, 2001.
14. C. Frohlich, "Total solar irradiance ...," *Space Science Reviews* **in press**, pp. xx–xx, 2001.
15. R. A. Barnes and C. R. McClain, "The calibration of SeaWiFS after two years on-orbit," *Proc. SPIE* **3870**, pp. 214–227, 1999.
16. A. P. Lane and W. M. Irvine, "Monochromatic phase curves and albedos for the lunar disk," *Astronom. J.* **78**, pp. 267–277, 1973.
17. P. Helfenstein and J. Veverka, "Photometric properties of lunar terrains derived from Hapke's equation," *Icarus* **72**, pp. 342–357, 1987.